

Electronic Supplementary Information

Field-effect transistor antigen/ antibody-TMDs sensors for the detection of COVID-19 samples

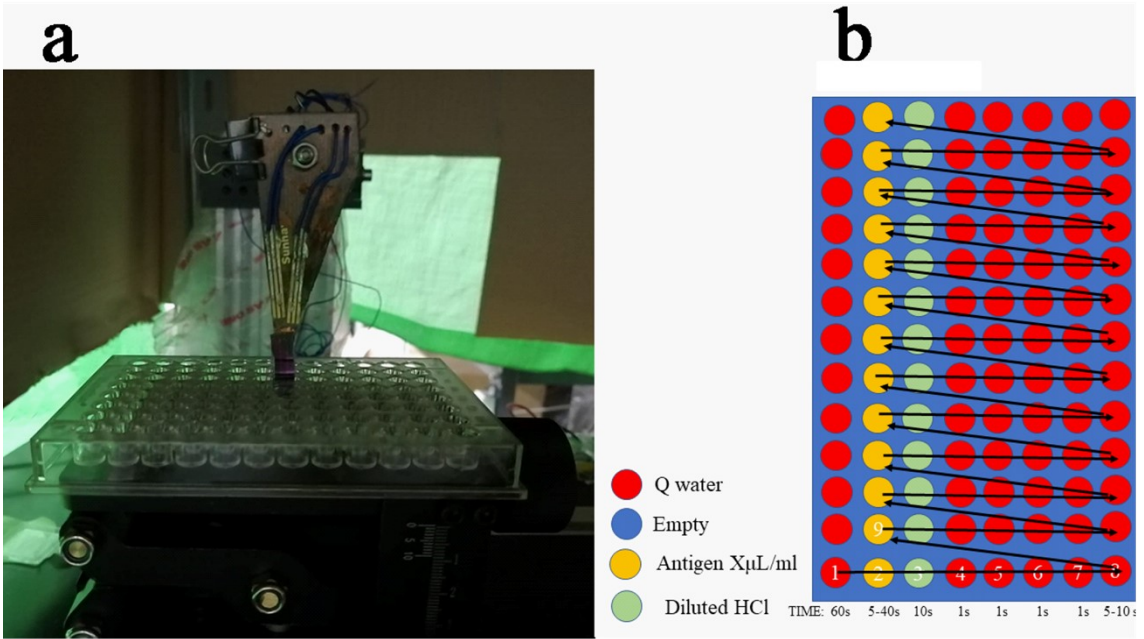
Ruben Canton-Vitoria,* Kotaro Sato, Yashiro Motooka, Shinya Toyokuni, Zeng Liu, Ryo Kitaura*

SUPPLEMENTARY EXPERIMENTAL SECTION

MoO₃, WO₃, S, Se, Te, NaCl, PPC, DPEA, DMAP, DCM, IPA, and MeOH were purchased from Sigma Aldrich with a purity of < 99.5 %. SARS-CoV-2/2019-nCoV Spike/S2 Antibody Rabbit PAb, Antigen Affinity Purified catalog number 40590-T62 and SARS-CoV-2 (2019-nCoV) Spike S2 ECD-His Recombinant Protein Cat: 40590-V08B was obtained by Sino Biological Inc. All the saliva was taken at a single time from a healthy volunteer and storage at -20 °C. Room-temperature PL spectra were measured by using a confocal Raman microscope (Renishaw InVia Raman and Horiba Jobin Yvon LabRAM HR-800) with 633 nm excitations. A notch filter was used to filter out Rayleigh scattering, and Raman and PL signals were detected with a charge-coupled device (CCD). An x 100 (0.8 NA) objective lens was used to focus the laser light on samples. Atomic force microscope (AFM) observations were performed by a Veeco AFM system (Dimension 3100SPM, Nanoscope IV) operated at a scanning rate of (0.1-1) Hz. High-resolution transmission electron microscopy (HRTEM) was performed on a JEOL JEM-2100F equipped with Energy Dispersive X-Ray (EDX) spectrometer, working at 80 keV. Steady-state UV-Vis-NIR absorption spectra were recorded on a PerkinElmer (Lambda 19) UV-Vis-NIR spectrophotometer. Lifetime measurements were carried out using a TCSPC module (SPC-130EM) and a single photon detector (ID-100-50-ULN) from Becker and Hickl GmbH. Fundamental properties, including transfer and output characteristics, of the transistors were measured using a Keithley semiconductor parameter analyzer (4200-SCS).

TEM grid preparation: A polypropylene carbonate (PPC) 15% in anisole film was spin-coated (5-seconds spinning at 1000 r.p.m followed by a 45-seconds coating at 6000 r.p.m) on a SiO₂ substrate with CVD-grown MoS₂ or WS₂; After heating at 135 °C for 1 minute, the SiO₂ substrate was soaked into water, and the PPC film was spontaneously separated from the substrate. The PPC film floating on the water surface was directly scooped up with a TEM grid. After drying at room temperature, the TEM grid was annealed at 135 °C for 1 minute. Finally, the PPC film was dissolved in acetone overnight, and the resulting TEM grid was heated at 100 °C in a vacuum for 30 minutes. After proper analysis. Functionalization employing the over-mentioned thiol reaction was employed.

AFM. Single layers of **1a** or **1b** were picked up by employing a drop of dry PPC on a SiO₂ transparent substrate. And then, a flake was transferred to a planar mechanically exfoliated multilayer hBN on SiO₂. The PPC was dissolved in acetone overnight and then completely purified using DCM under Solhex reflux. Lately, it has been functionalized and carefully studied by PL and AFM analysis before and after functionalization.



Scheme S1. (a) Optical picture of the system and (b) experiment in 96-grids ELISA plate Scheme.

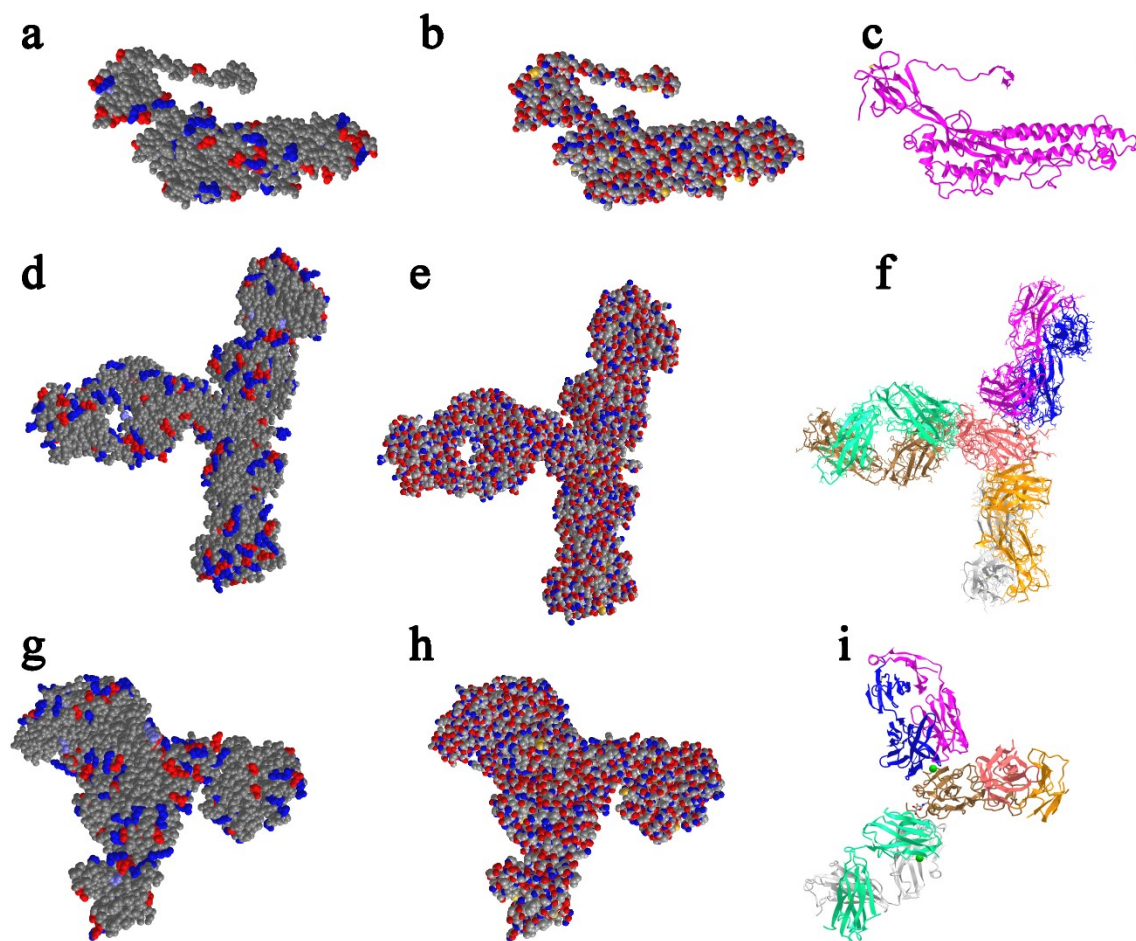


Figure S1. (a-c) antigen, (d-i) antibodies. (a, d, g) red and blue charged regions of the antigen or antibodies. Negative density areas are in blue, positive density areas are in red. (b, e, h) red, blue and yellow represent oxygen, nitrogen, and sulfur. (c, f, and i) each chain shown is by different colors, and spheres correspond to ions. Structural information was taken from YP_009724390.1 and Ser686-Pro1213.ⁱ Random Spike antibodies are from PDB ID: 7JX3_Bⁱⁱ and 7R6X_Cⁱⁱⁱ, respectively.

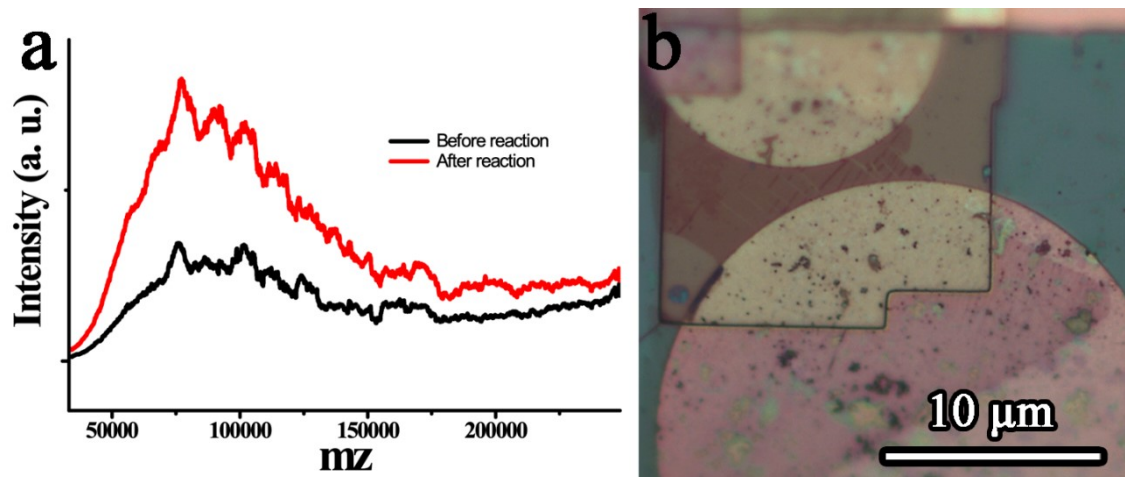


Figure S2. (a) MALDI of antibody before the reaction (black) and antibody after the reaction (red) with MoS₂. (b) Degradation of MoS₂ layers in FET-devices after several cleanings of Van der Waals non-covalent functionalization of FET antibodies-MoS₂ by the superficial tension of water.

Structural characterizations

AFM images show that antibodies are attached to the whole surfaces, including MoS₂, SiO₂, and electrodes via covalent bonding and/or van der Waals interactions. Our antibodies are polyclonal and various antibody sizes (bubbles of 30-100 nm) are observed. Single layers of MoS₂ are thinner than 1 nm (Fig. S3a) and are hardly distinguishable after adding antibodies (Fig. S3a and b vs S3c-d); No breaks of the MoS₂ flakes or electrodes have been seen. Magnification of figure S3c in S3d shows the characteristic bubble shape of antibodies.^{iv}

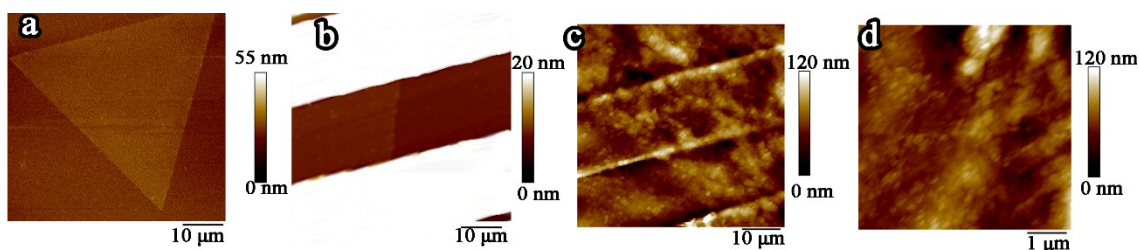


Figure S3. AFM images of (a) MoS₂ (b) FET of MoS₂, (c) FET antibody-MoS₂ and (d) magnification of (c) on basal plane of MoS₂-Antibody, without the interference of electrodes.

Raman spectra of CVD-grown MoS₂ ensured a semiconducting phase since J₁, J₂, and J₃, which appear only in the metallic phase were absent. Positions of A_{1g} and E_{12g} (407 and 381 cm⁻¹) are consistent with pristine semiconducting-phase MoS₂. Very importantly, 2LA(M) band associated with the number of defects can also be seen at 450 cm⁻¹. Addition of thiols in vacancies of Sulphur (covalent functionalization) decrease the number of defects, proving the covalent functionalization.^{v,vi,vii,viii,ix} No additional Raman band exists, ensuring the absence of possible impurities like NaCl or MoO₃. After functionalization, the E_{12g}/A_{1g} and 2LA(M)/A_{1g} ratio significantly decreases by 20 and 8 % respectively, indicating a strong interaction between MoS₂ and cysteines of antibodies (see Fig. S4 a). Concretely, 2LA(M) reduction suggests the addition of cysteine to Sulphur vacancies of MoS₂. E_{12g} and A_{1g} are shifted 2 and 1 cm⁻¹ to lower and higher energies, respectively. In addition, Raman bands of antibodies appear between 1000-2000 cm⁻¹ and 2700-3500 cm⁻¹, which can be attributed to the α - Helix and aromatic chains (see Fig. S4 b). Raman mapping shows homogeneous distribution over the MoS₂ and remains unaltered after functionalization (Fig. S4c). Also, the intensity of antibody is uniform over the whole device (Fig. S4d), which agrees with AFM images.

XPS was problematic in antibody-MoS₂. Due to the high power of the laser the antibodies degrade, and unreal information is recorded. However, thiol derivatives in figures S4e and f modify the binding energies of MoS₂. 0.15 and 0.10 eV shift to higher binding energies of Sulphur 2P_{1/2} and 2P_{3/2} in figure 4e suggest a decreasing of Sulphur vacancies,^{xxi} suggesting covalent functionalization.

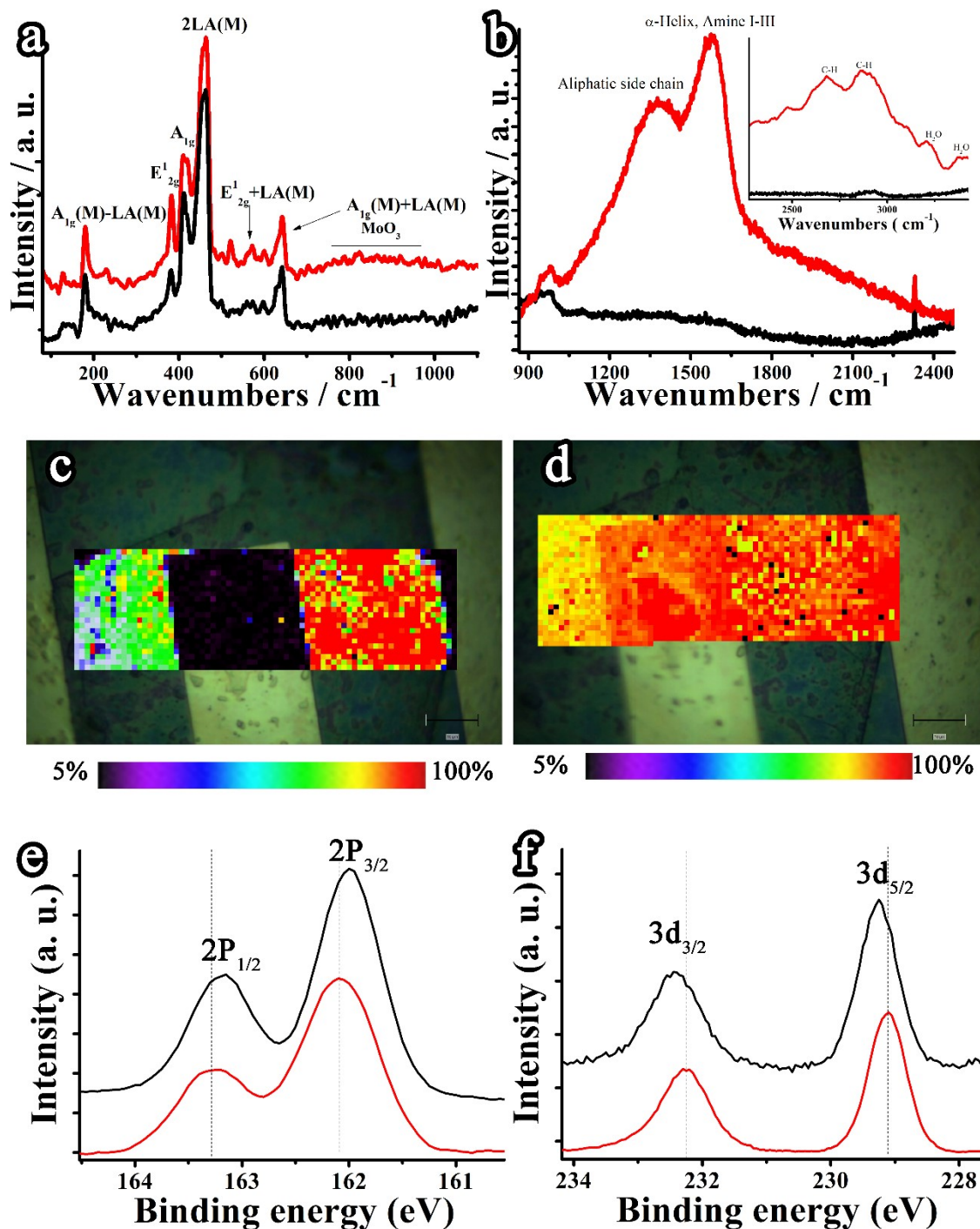


Figure S4. (a, b, and b-inset) Raman spectra measured with the excitation wavelength of 633 nm of (black) MoS₂ and (red) Antibody-MoS₂. Raman intensity mapping of (c) E_{2g}¹+A_{1g} modes of MoS₂ and (d) C-H aliphatic chain of FET antibody-MoS₂ device. XPs of (e) Sulphur and (f) Molybdenum for pristine MoS₂ (black) and Thiol-MoS₂ (red)

TEM images of antibody-MoS₂ were unclear because the thick antibodies mask the image contrasts of MoS₂ (see Fig. S5b). However, we include low magnifications TEM figures after functionalization showing that the layers of MoS₂ are stable during the functionalization process (see Fig. S5c). It is obvious that the edges of the layers have higher amount of functionalization than basal plane. It is because the most stable edges are zig-zag terminated Mo atoms (zz-Mo). Naked atoms of Mo are very reactive and easily interact with cysteines, increasing the level of functionalization with antibodies at

the edges.^{xii,xiii,xiv} In contrast, Fig. S5a shows TEM images of pristine MoS₂ with atomic resolution. The crystallinity is consistent with semiconducting 2H-MoS₂. We also observed defects on basal plane of pristine MoS₂, highlighted with arrows in Fig. S5a; In those defective position we expected that the antibodies would be anchored after functionalization.

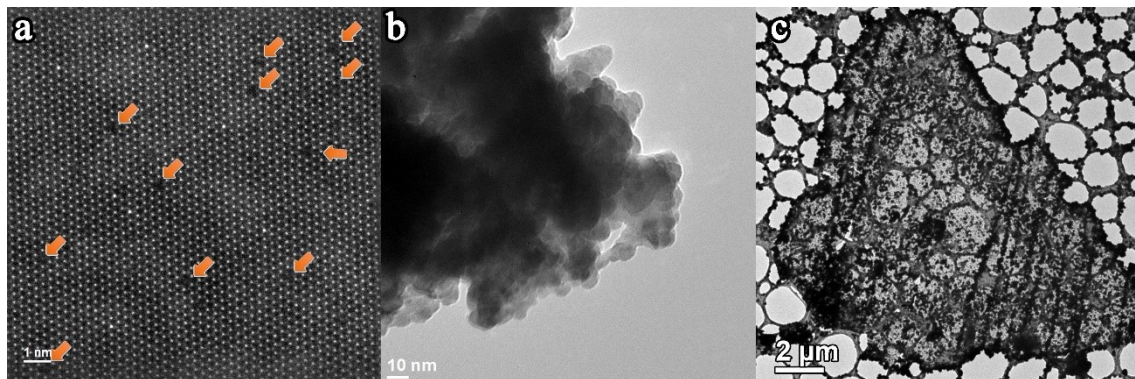


Figure S5. TEM images of (a) a pristine CVD-grown MoS₂ and (b) Antibody-MoS₂ and (c) low magnifications of Antibody-MoS₂.

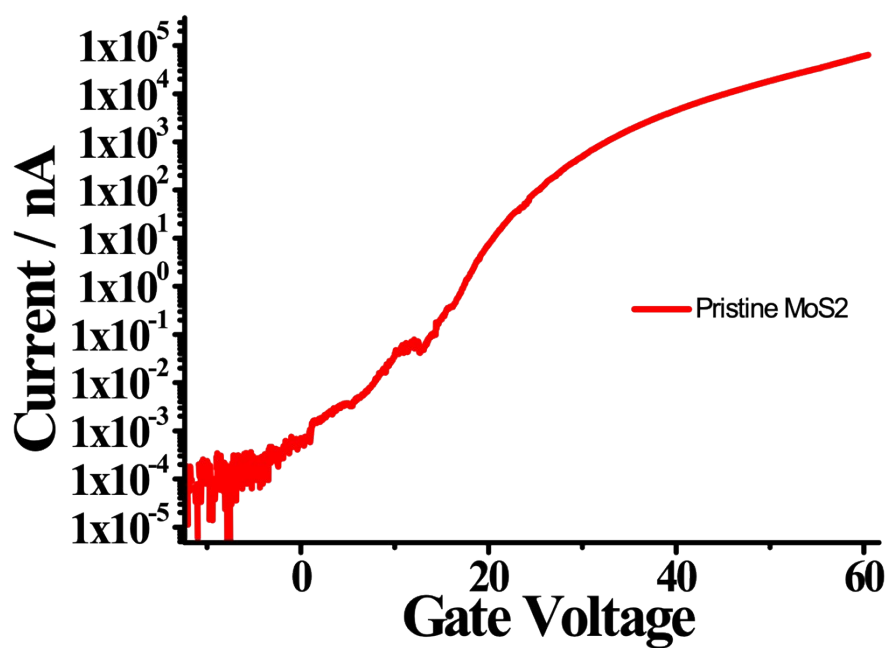


Figure S6. Transfer curve of 1 single layer of MoS₂-based FET device with Bi/Au electrodes. Experiment was carried out at 1 V_{DS} in air.

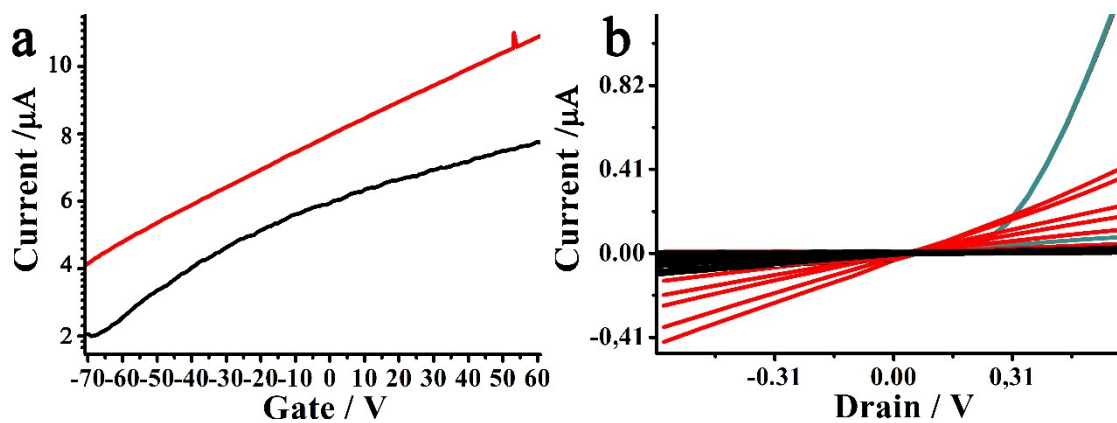


Figure S7. (a) Transfer curves at 0.5 V_{DS} and (b) output characteristics of FET-antibody-MoS₂ with (black) and without (red) antigen under a variation of 10 V_G (-60 to 60V). The green lines correspond to MoS₂ before covalent functionalization with antibody. These experiments were carried out in air.

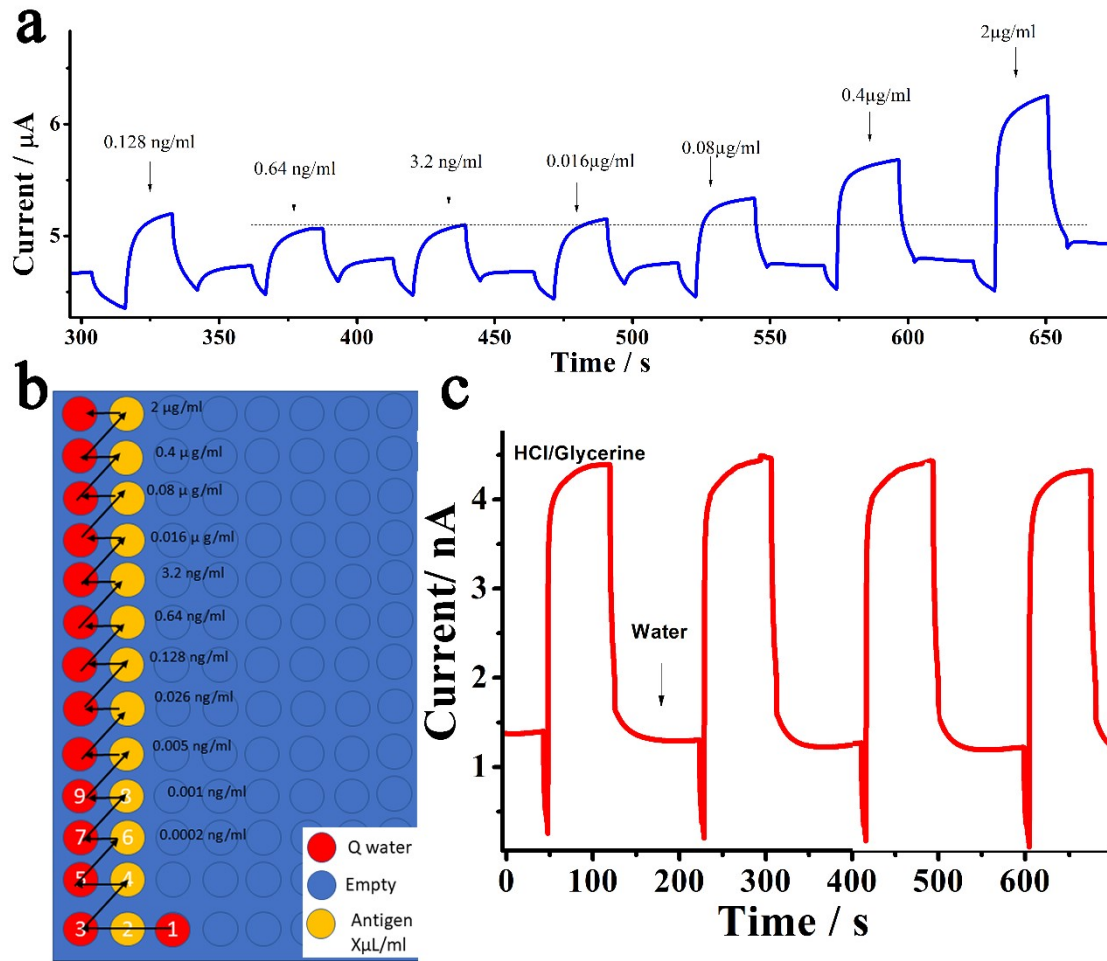


Figure S8. (a) Additions of antigen to FET MoS₂ blank device in a crescent concentration of antibodies. (b) Process carried out in (a). (c) FET antibody-antigen black device under exchange of water and HCl/Glycerine. All experiments were carried out at 0.5 V_{DS} and 0 V_G.

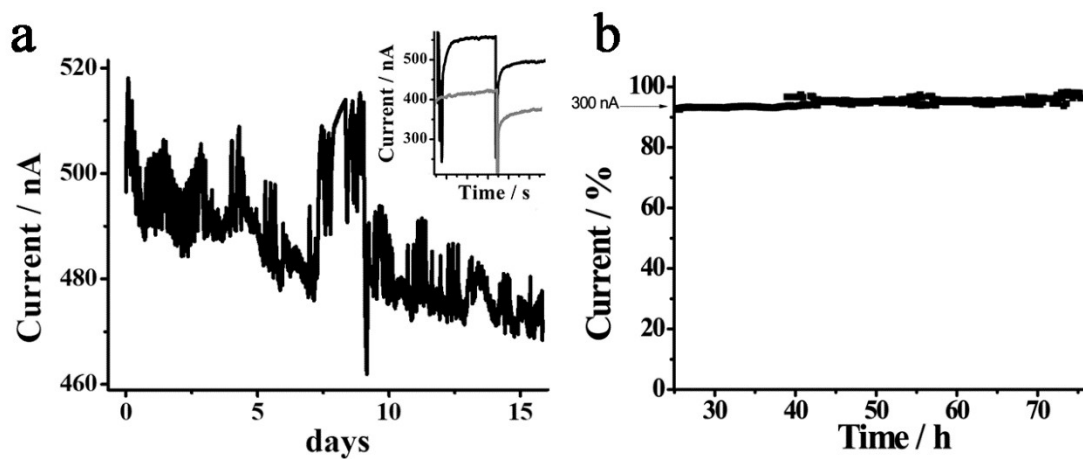


Figure S9. Stability of FET Antibody-MoS₂ in (a) air and (b) water under drain to source voltage of 0.5 V and gate voltage of 0V. **Note:** Temperature changes are responsible for the slight change in the baseline. Inset of (a): Changes of the current after interaction with antigen on first day (black) and after 15 days (gray). The experiment was carried out under drain to source voltage of 0.5 V, gate voltage of 0V and concentrations of 50 pg/ml S2 glycoprotein.

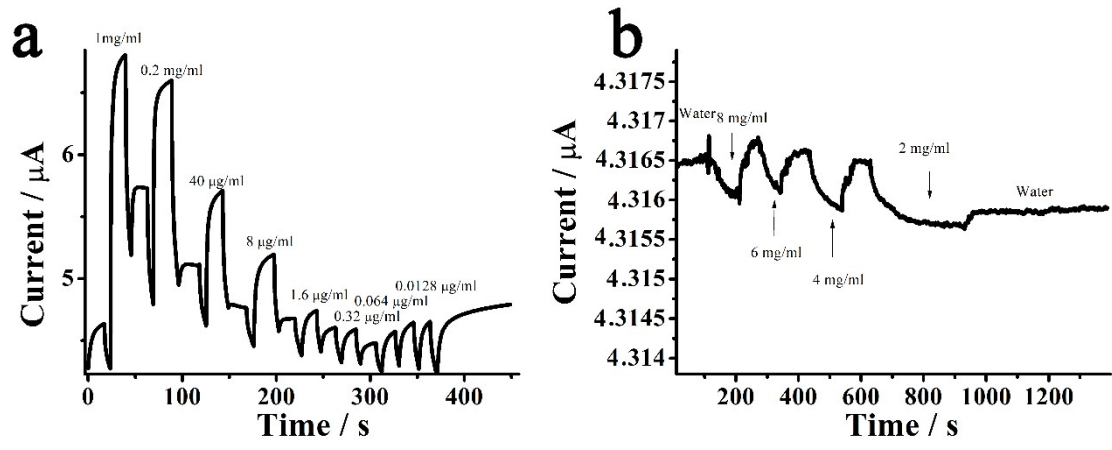


Figure S10. Additions of NaCl to FET devices of MoS₂ previous (a) and after (b) addition of antibodies at different concentrations of antigen. All experiments were carried out at $0.5 V_{DS}$.

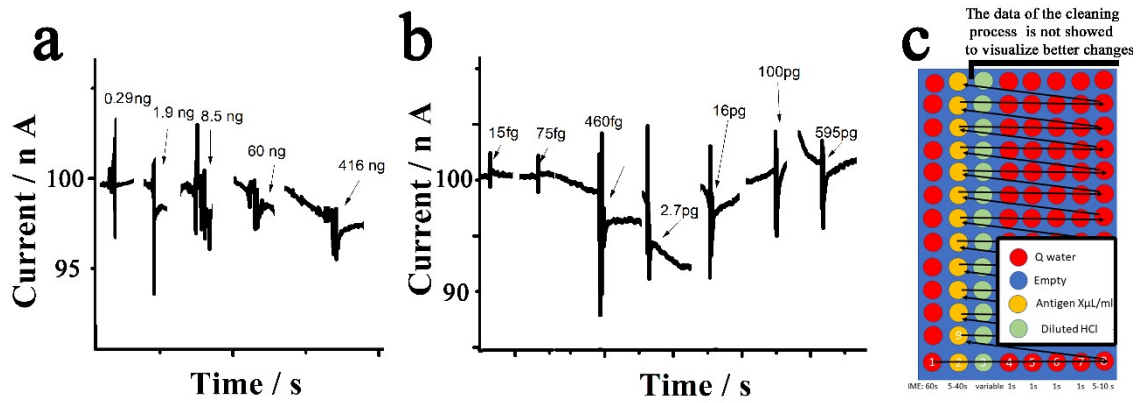


Figure S11. Crescent additions of (a) KLH and (b) Albumin to antibody- MoS₂ based devices. Current and time are not real in this experiment and cleaning process has been cut it to better visualization of the data. All experiments were carried out at 0.5 V_{DS}. (c) Experiment in 96-grids ELISA plate Scheme.

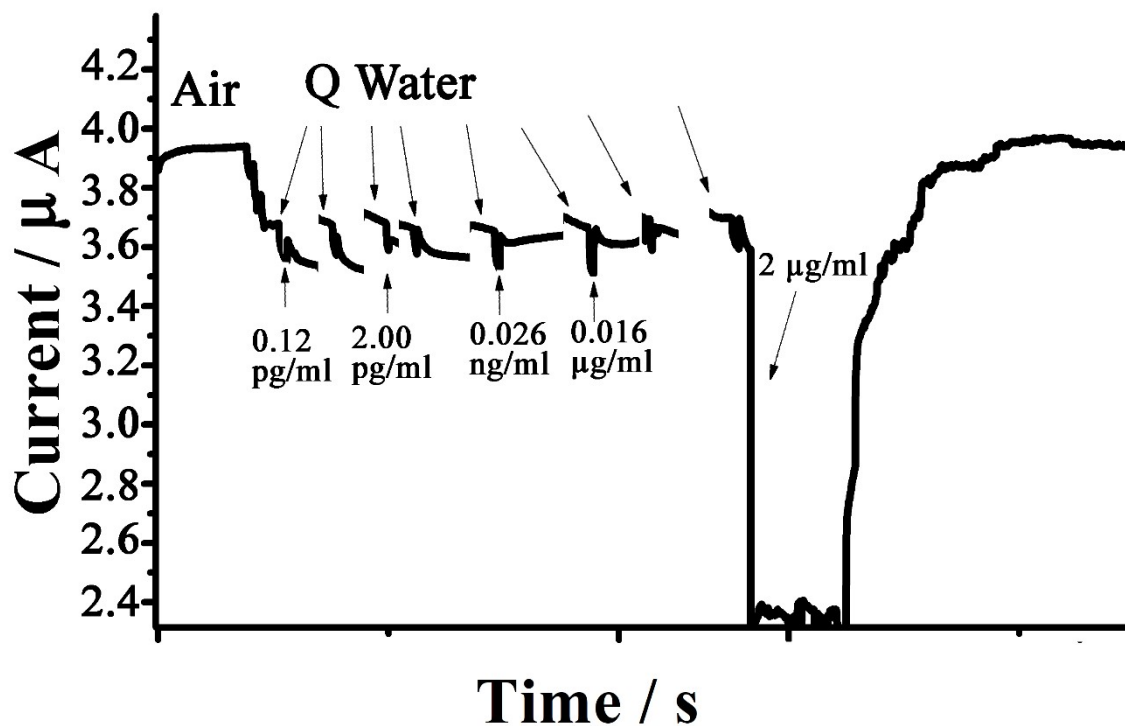


Figure S12. Additions of antigen to FET Antibody-WS₂ device in a mixture of saliva/water 50%/50% solutions. Current and time are not real in this experiment. Cleaning process has been cut to better visualization of the data. All experiments were carried out at 0.5 V_{DS}.

References

- ⁱ Wu, F.; Zhao, S.; Yu, B.; Chen, Y.; Wang, W.; Song, Z.; Hu, Y.; Tao, Z.; Tian, J.; Pei, Y.; Yuan, M.-L.; Zhang, Y.-L.; Dai, F.-H.; Liu, Y.; Wang, Q.-M.; Zheng, J.-J.; Xu, L.; Holmes, E. C.; Zhang, Y.-Z.; A new coronavirus associated with human respiratory disease in China. *Nature* 2020, **579**, 265. PDB ID: 7fG7
<https://doi.org/10.1038/s41586-020-2008-3>
- ⁱⁱ Piccoli, L.; Park, Y.; Tortorici, M.; Czudnochowski, N.; Walls, A.; Beltramello, M.; Silacci-Fregni, C.; Pinto, D.; Rosen, L.; Bowen, J.; Acton, O. J.; Jaconi, S.; Guarino, B.; Minola, A.; Zatta, F.; Sprugasci, N.; Bassi, J.; Peter, A.; Veessler.; Mapping neutralizing and immunodominant sites on the SARS-CoV-2 spike receptor-binding domain by structure-guided high-resolution serology. *Cell* 2020, **183**, 1024. PDB ID 7JX3_B:
<https://doi.org/10.1016/j.cell.2020.09.037>
- ⁱⁱⁱ Starr, T.; Czudnochowski, N.; Liu, Z.; Zatta, F.; Park, Y.; Addetia, A.; Pinto, D.; Beltramello, M.; Hernandez, P.; Greaney, A. J.; Marzi, R.; Glass, W. G.; Zhang, I.; Dingens, A. S.; Bowen, J. E.; Tortorici, M. A.; Walls, A. C.; Wojcechowsky, J. A.; Marco, A. D.; Rosen, L. E.; Zhou, J.; Montiel-Ruiz, M.; Kaiser, H.; Dillen, J. R.; Tucker, H.; Bassi, J.; Silicci-Fregni, C.; Housley, M. P.; Lulio, J. D.; Lombardo, G.; Agostini, M.; Sprugasci, N.; Culap, K.; Jaconi, S.; Meury, M.; Dellota, E.; Adbelnabi, R.; Foo, S.-Y. C.; Cameroni, E.; Stumpf, S.; Croll, T. I.; Nix, J. C.; Havenar-Daughton, C.; Piccoli, L.; Benigni, F.; Neyts, J.; Telenti, A.; Lempp, F. A.; Pizzuto, M. S.; Chodera, J. D.; Herbner, C. M.; Virgin, H. W.; Whelan, S. P.J.; Veessler, D.; Corti, D.; Bloom, J. D.; Snell, G.; SARS-CoV-2 RBD antibodies that maximize breadth and resistance to escape. *Nature* 2021, **597**, 97. PDB ID 7R6X_C:
<https://doi.org/10.1038/s41586-021-03807-6>
- ^{iv} Hu, J.; Gao, M.; Wang, Z.; Chen, Y.; Song, Z.; Xu, H.; Direct imaging of antigen–antibody binding by atomic force microscopy. Direct imaging of antigen–antibody binding by atomic force microscopy. *Appl. Nanosci.*, 2021, **11**, 293–300
<https://doi.org/10.1007/s13204-020-01558-w>
- ^v Canton-Vitoria, R.; Gobeze, H. B.; Blas-Ferrando, V. M.; Ortiz, J.; Jang, Y.; Fernández-Lázaro, F.; Sastre-Santos, Á.; Nakanishi, Y.; Shinohara, H.; D'Souza, F.; Tagmatarchis, N.; Excited-state charge transfer in covalently functionalized MoS₂ with a Zinc phthalocyanine donor–acceptor hybrid. *Angew. Chem.* 2019, **131**, 5768.
<https://doi.org/10.1002/anie.201900101>
- ^{vi} Canton-Vitoria, R.; Scharl, T.; Stergiou, A.; Cadranel, A.; Arenal, R.; Guldi, D. M.; Tagmatarchis, N.; Ping-pong energy transfer in covalently linked porphyrin-MoS₂ architectures. *Angew. Chem. Int. Ed.* 2020, **59**, 1, 3976.
<https://doi.org/10.1002/anie.201914494>
- ^{vii} Canton-Vitoria, R.; Istif, E.; Hernández-Ferrer, J.; Urriolabeitia, E.; Benito, A.; Maser, W.; Tagmatarchis, N.; Integrating water-Soluble polythiophene with transition-metal dichalcogenides for managing photoinduced processes. *ACS Appl. Mater. Interfaces* 2019, **11**, 5947.
<https://doi.org/10.1021/acsami.8b18435>
- ^{viii} 29- Vallan, L.; Canton-Vitoria, R.; Gobeze, H. B.; Jang, Y.; Arenal, R.; Benito, A. M.; Maser, W. K.; D'Souza, F.; Tagmatarchis, N.; Interfacing transition metal dichalcogenides with carbon nanodots for managing photoinduced energy and charge-transfer processes. *J. Am. Chem. Soc.* 2018, **140**, 13488.
- ^{ix} 31- Canton-Vitoria, R.; Vallan, L.; Urriolabeitia, E.; Benito, A. M.; Maser, W. K.; Tagmatarchis, N.; Electronic interactions in illuminated carbon dot/MoS₂ ensembles and electrocatalytic activity towards hydrogen evolution. *Chem. Eur. J.* 2018 **24**, 10468.
<https://doi.org/10.1002/chem.201801425>
- ^x Canton-Vitoria, R.; Sayed-Ahmad-Baraza, Y.; Pelaez-Fernandez, M.; Arenal, R.; Bittencourt, C.; Ewels, P. C.; Tagmatarchis, N.; Functionalization of MoS₂ with 1,2-dithiolanes: toward donor-acceptor nanohybrids for energy conversion. *npj 2D Mater. Appl.* 2017, **1**, 1.
<https://doi.org/10.1038/s41699-017-0012-8>
- ^{xi} Canton-Vitoria, R.; Sayed-Ahmad-Baraza, Y.; Arenal, R.; Ewels, C. P.; Tagmatarchis, N.; Pyrene-functionalized tungsten disulfide as stable resistive photosensor. *Mater. advances* 2020, **10**, 363.
[10.1039/d0ma00429d](https://doi.org/10.1039/d0ma00429d)

^{xii} Zhou, H.; Yu, F.; Liu, Y.; Zou, X.; Cong, C.; Qiu, C.; Yu, T.; Yan, Z.; Shen, X.; Sun, L.; Yakobson, B.; Tour, J.; thickness-dependent patterning of MoS₂ sheets with well-oriented triangular pits by heating in air. *Nano Res.* 2013, **6**, 703.

<https://doi.org/10.1007/s12274-013-0346-2>

^{xiii} Lv, D.; Wang, H.; Zhu, D.; Lin, J.; Yin, G.; Lin, F.; Zhang, Z.; Jin C.; Atomic process of oxidative etching in monolayer molybdenum disulfide. *Sci. Bull.* 2017, **62**, 846.

<https://doi.org/10.1016/j.scib.2017.05.016>

^{xiv}I. de Castro, R.; Datta, J.; Ou, A.; Castellanos-Gomez, S.; Sriram, T.; Daeneke, K.; Kalantar-zadeh; Molybdenum Oxides – From Fundamentals to Functionality. *Adv. Mater.* 2017, **29**, 40, 1.

<https://doi.org/10.1002/adma.201701619>